EASR

Engineering and Applied Science Research

https://www.tci-thaijo.org/index.php/easr/index

Published by the Faculty of Engineering, Khon Kaen University, Thailand

Characterization and mechanical properties of AA1100 aluminium alloy coated on a metakaolin substrate produced by the spot friction surfacing process

Sukangkana Talangkun*[1)] and Dhammasook Mingmuang[2)]

[1)]Department of Industrial Engineering, Faculty of Engineering, Khon Kaen University, Khon Kaen, Thailand
[2)]Faculty of Science and Engineering, Kasetsart University, Chalermphrakiat Sakon Nakhon Province Campus, Thailand

Received 23 November 2021
Revised 26 April 2022
Accepted 9 May 2022

Abstract

The aim of this research was to demonstrate the properties of a thin, high purity aluminium AA1100 layer coated on a metakaolin substrate deposited using a spot friction surfacing process. Under the coating parameters, an AA1100 layer continuously adhered to a metakaolin substrate. Cracking of the substrate was not observed. Although surface roughness (Rz) of metakaolin at the Al/Metakaolin interface was reduced by 15.66% after friction surfacing, mechanical interlocking can be observed. There was no evidence of macro-or micro-cracking on the post-process substrate. The electrical resistance values were uniform in all directions. The average thickness of the AA1100 coating layer was less than 1 micron. After processing, both the average hardness and the modulus of the AA1100 coating layer increased. Furthermore, the maximum temperature during the process measured by infrared thermography was lower than the AA1100 recrystallization temperature. Compression residual stress on the AA1100 coating layer, estimated using an X-ray diffraction method, was-27.20 MPa.

Keywords: Aluminium AA1100, Metakaolin, The spot friction surfacing process, Solid-state joining

1. Introduction

Packaging of the power electronics modules used in high temperature environments is rapidly developing. For high temperature operation, high electrical conductivity of metal bonded ceramic substrates is required for power electronics modules [1, 2]. Due to their high thermal conductivity, electrical conductivity and high melting point, direct bonded copper (DBC) coatings have been the most promising for packaging of power electronics modules [3-5]. However, cracking of DBC coatings, delamination of copper caused by thermal stress [6] and thermal cyclic loads [7, 8] are major problems. A low-yield strength material has become an alternative to producing interconnected metal to reduce thermal stress [9, 10]. Aluminium and its alloys were the first examined because of their low-yield strength with good thermal and electrical conductivity. For this reason, the direct-bonded aluminium (DBA) coatings were developed [11, 12].

There have been many methods used for coating ceramics with layers of metal. For example, physical vapor deposition and chemical vapor deposition were used to produce copper films on a ceramic for an IGBT module [13, 14]. However, the cost of the process was rather high. Even though liquid state joining and soldering have been widely used, the complexity of these coating processes still remains their main disadvantage [15, 16]. The possibility of solid-state joining methods, such as hot pressing, seems only applicable as a metal/ceramic coating process, since the wettability between a hot viscous metal and a ceramic is relatively high [17]. Recently, a coating of 99.9 wt% high-purity aluminium on a ceramic was successful performed using a hot press method [5]. The bonding mechanism in solid-state joining of a metal/ceramic interface was dominated by mechanical interlocking and diffusion bonding. For this reason, the bonding strength of the metal/ceramic interface *via* solid-state joining was rather high. Furthermore, a friction-based joining process producing high bonding strength, used by earlier researchers to join metal/metal materials, was applied to join metal/ceramics [18-20]. Another interesting process is the friction surfacing operation. It was developed from friction welding to coat a metal onto another metal surface [21]. In metal/metal friction stir welding, the thermo-mechanically affected zone (TMAZ), which is a transition zone between the stir zone (SZ), and the heat affected zone (HAZ), have crucial roles in developing weld strength. It has been shown that a TMAZ was not observed in copper and was hardly found in 5083 aluminium alloys after friction stir welding using various rotational speeds [22]. A small TMAZ of an aluminium rod improves weld strength. From the processing point of view, the friction process is simpler, cost effective and has a lower energy consumption than hot pressing. So, it is a promising process to apply a direct-bonded aluminium (DBA) coating.

Additionally, the friction surface between aluminium and a ceramic has been successfully applied for fabrication of thermoelectric cells [23]. An AA1100 alloy was successfully coated on a metakaolin substrate using a spot friction surfacing process. This is a promising process for producing metal/ceramic thermoelectric devices. Currently, there is limited knowledge of the microstructure and mechanical properties of this metal/ceramic coating. Therefore, the aim of this work is to demonstrate a spot friction surfacing process developed from the friction surfacing process of the DBA coating for power electronics modules and other electronic devices.

*Corresponding author. Tel.: +66 4300 9700 ext. 45632
Email address: Sukangkana@kku.ac.th
doi: 10.14456/easr.2022.59

Metakaolin was chosen as the substrate. Consumable rods made from Aluminium AA1100 were used. The process temperature, electrical resistance and mechanical properties of the coated layer were studied. Substrate surface conditions were also investigated to evaluate the wear of the substrate caused by friction.

2. Experimental procedure

2.1 Materials

A 5 mm diameter annealed aluminium AA1100 rod was used as a consumable material. A sintered metakaolin plate was prepared with the dimensions of 25.4 mm × 25.4 mm × 1 mm and used as the substrate. Chemical composition of the aluminium rod and metakaolin substrate were spectrophotometrically analyzed. These results are presented in Tables 1 and 2, respectively. It should be noted that the presence of Mn, Si and Fe results as a response to strain hardening.

2.2 The spot friction surfacing process

The spot friction surfacing process was performed on a CNC milling machine (Model HASS VCE 750, USA). An AA1100 rod was rotated and simultaneously pressed on a sintered metakaolin substrate. The spot friction surfacing conditions were a rotation speed of 7500 rpm, axial feed rate of 0.3 mm/min (approximately 5 microns per second) and depth of cut of 50 microns. Once a rod was pressed onto the substrate, it was held for 10 sec. A schematic of the spot friction surfacing process is given in Figure 1a. The temperature of the aluminium consumable rod induced by friction was measured using an infrared thermographic camera (Fluke Ti400, USA), as shown in Figure 1b. The aluminium consumable rod was anodized and dyed in matte black to produce a black body material with an emissivity as close to 1.00 as possible. This was done for infrared thermographic measurements [24]. The condition for temperature measurement included a background temperature of 26 °C, transmission of 100%, and a distance to target of 10 cm.

Table 1 Chemical composition of an AA1100 consumable rod.

Al 1100	Al	Zn	Cu	Mn	Si+Fe	Other, each	Other, total
Standard	≥ 99 %	≤ 0.1 %	≤ 0.05 %	≤ 0.95 %	0.05 - 0.2 %	≤ 0.05 %	≤ 0.15 %
Rod	99.3	0.01	0.12	0.007	0.48	-	0.072

Table 2 Chemical composition of a metakaolin substrate.

Element	SiO_2	Al_2O_3	Fe_2O_3	MgO	CaO	Na_2O	K_2O	TiO_2	Loss of ignition
%	54.5	33.9	0.24	0.25	0.65	1.66	1.96	0.02	6.09

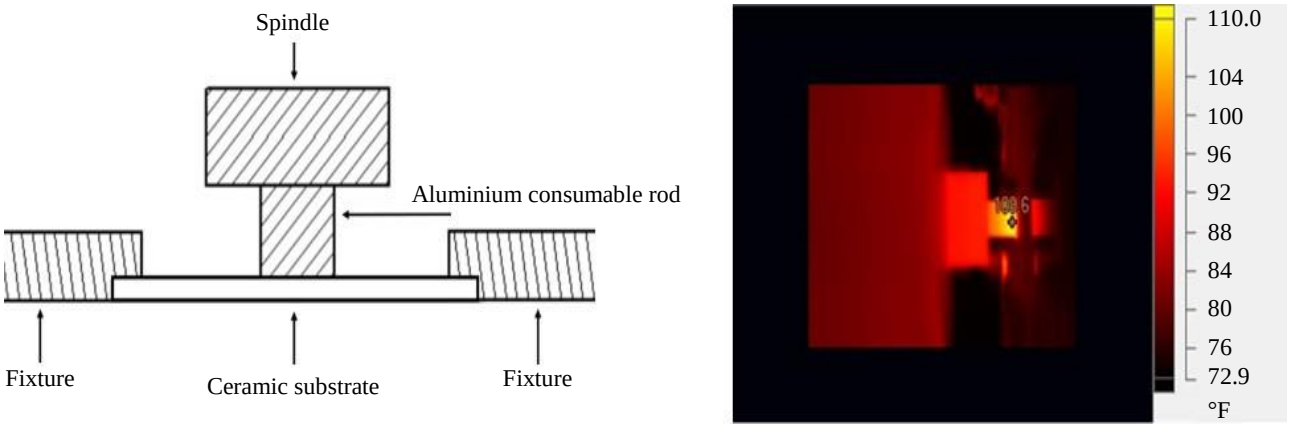

(a) (b)

Figure 1 (a) Schematic of the spot friction surfacing process, (b) Temperature measurement using infrared thermography.

2.3 Metallography

The macrostructure of the coated layer was inspected using a stereo microscope. For surface analysis, field emission scanning electron microscopy (FESEM) was performed on the substrate's surface. Additionally, the thickness of the coated layer was measured using focused ion beam and field emission scanning electron microscopy (FIB-FESEM).

2.4 Properties of the coating layer

2.4.1 Electrical resistance of the aluminium coated layer

To measure electrical resistance, the coated sample was made in the form of overlapping spots, as shown in Figure 2. A Pico test was performed across the overlapping layer of 2 spots in 10 lines, including C-1, D-C, D-1, B-D, B-C, B-1, A-1, A-D, A-C, and A-B, of the 2 spots overlap, as presented in Figure 2.

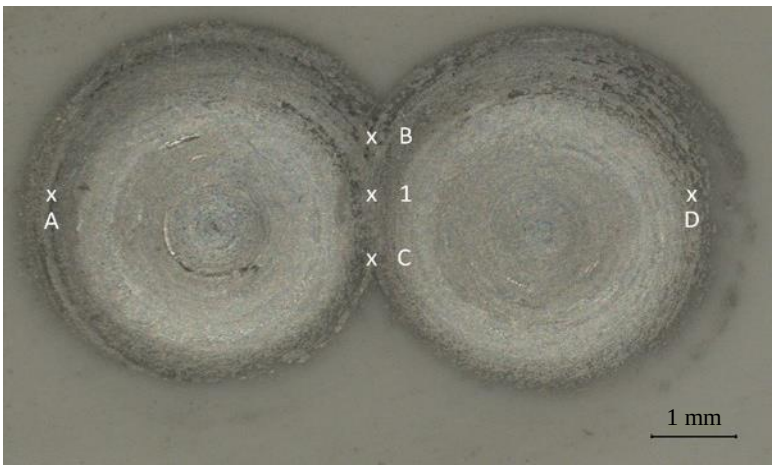

Figure 2 The locations of the electrical resistance measurement.

2.4.2 Nanohardness and modulus

A nanoindentation test was performed to measure the hardness of the coating layer using a Hysitron Ti Premier (Bruker, USA). A 1 mN load was applied and the mean contact depth was approximately 200 nm. After that, the Young's modulus of the AA1100 coating layer and the initial AA1100 were calculated using Equation (1) [25].

$$E_i = \frac{1 - v_i^2}{E_r^{-1} - [(1 - v_s^2)/E_s]} \quad (1)$$

where v_s is the Poisson's ratio of the indenter (diamond = 0.18), v_i is Poisson's ratio of aluminium AA1100 (0.33) [26], E_s is Young's modulus of the indenter (diamond = 1,050 GPa) [27] and E_i is the Young's modulus of the AA1100. E_r is the Reduced Young's modulus of aluminium. The measured value of E_r from the indentation for the AA1100 and the coated layer were 71.77 and 73.19 MPa, respectively.

2.4.3 Estimation of residual stress of the aluminium coating layer

Diffraction of the coating layer was measured using synchrotron X-ray diffraction to estimate residual stress. The beam power was 12,000 eV. The spot size of the beam was 0.3 mm x 3 mm. Exposure time was 1,000 sec. The incident angles were 10°, 14° and 22°. A schematic of the measurement setup is shown in Figure 3. Calculation of residual stress followed the conventional d-sin$^2\Psi$ mode [28]. After the diffraction measurements were made, 2θ angles and the intensity of the incident angle were plotted and aligned to the reference of alumina (JCPDS 00-046-1212). This step was used to identify the peak of aluminium. Due to high energy intensity, the planes chosen for examination were 100, 200 and 311. After that, $d_{\{hk1\}}$ values obtained from various incident angles were calculated using Equation (2). Additionally, Ψ values obtained from various incident angles were also determined from Equation (3). In terms of the lattice plane, sin^2 Ψ values and $d_{\{hk1\}}$ values were plotted together. Then, the slope and y-intercept were identified. Finally, the residual stresses were calculated from Equation (4).

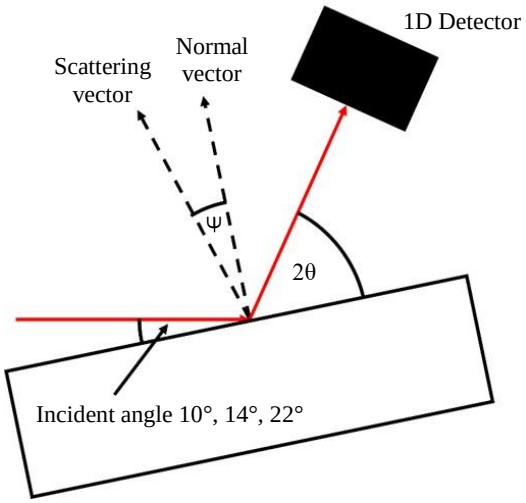

Figure 3 A schematic diagram of X-ray diffraction (XRD) measurements.

$$d_{hkl} = \frac{n\lambda}{2sin\theta} = \frac{a}{\sqrt{h^2 + k^2 + l^2}} \quad (2)$$

$$\psi = \theta - incident\ angle \tag{3}$$

$$\sigma = \frac{EC}{D(1+\upsilon)+(2\upsilon C)} \tag{4}$$

where $a_{\{hk1\}}$ are the lattice parameters, λ is a constant for copper, k_α = 0.15459, d_{hk1} is the d-spacing, C is the slope, D is the y-intercept, E is the Young's modulus of the aluminium coated layer obtained from Equation (1) = 68.48 GPa, υ = Poisson's ratio for aluminium (0.33) [26], and σ = residual stress (GPa).

2.5 Surface roughness of the metakaolin substrate

To estimate wear of the substrate after friction, the average maximum height of the roughness profile or Rz was measured and interpreted as the level of failure after friction surfacing. The overlapping specimen spots were soaked in an NaOH solution for 8 hours to remove the aluminium coating layer. After that, the exposed surface was subjected to a roughness test using a Mitutoyo SURFTEST SJ-310 (Mitutoyo, Japan). Each presented result is the average of three measurements. Each measurement line was 9 mm long. An illustration of the measurements performed is shown in Figure 4.

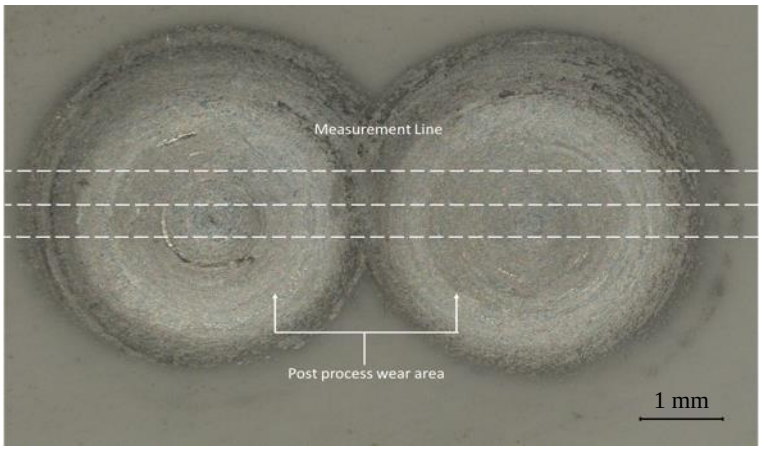

Figure 4 Illustration of Rz measurements.

3. Results and discussion

3.1 Thermomechanical process and process temperature

From preliminary experiments of this study, adhesion between the AA1100 alloy and metakaolin substrate did not occur at rotation speeds lower than 3,500 rpm. Although deformation of AA1100 occurred by a thermomechanical process [29-31], slippage of the AA1100 alloy did not occur. The shear stress between a consumable rod and a metakaolin substrate was insufficient. Additionally, macro-cracking occurred with axial feed rates greater than 0.6 mm/min. Therefore, a rotation speed of 7,500 rpm was chosen to ensure sufficient shear stress. An axial feed rate of 0.3 mm/min and a 0.3 mm depth of cut were used.

The macrostructure of aluminium coated on a metakaolin substrate by the spot friction surfacing process is presented in Figure 5a. The diameter of the aluminium coated layer was about 3 mm. Spot friction processing was successful in coating the metakaolin with AA1100 with no cracking. The coating layer adhered to the metakaolin substrate. Therefore, a processing time of 10 sec was sufficient. In Figure 5b, the FESEM image shows slippage of viscous aluminium that adhered to the metakaolin substrate.

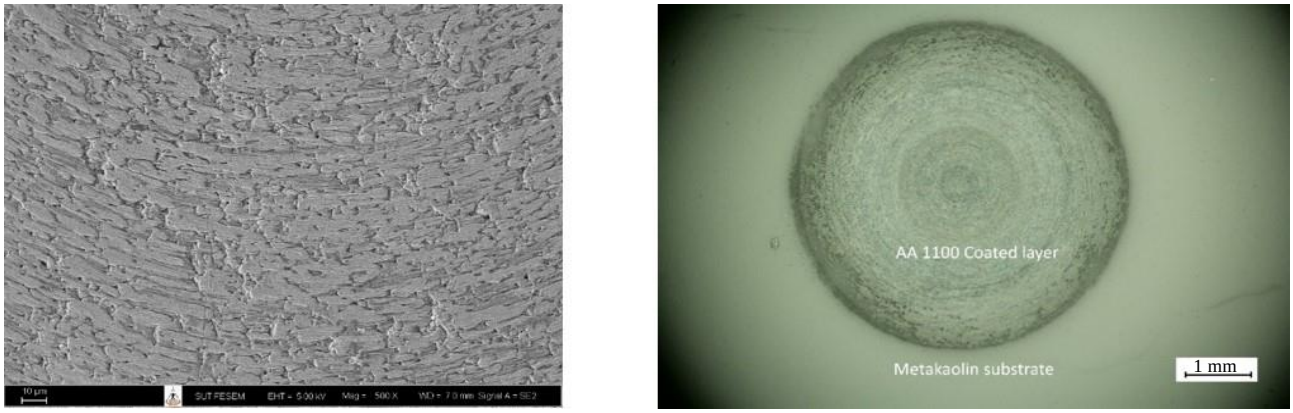

(a) (b)

Figure 5 (a) Macrostructure of a coating layer that was formed using the spot friction surfacing process, (b) FESEM Image of the surface of the AA1100 coated layer.

Using the FIB-FESEM technique, the thickness of the coated layer is as presented in Figure 6a, where a AA1100 coating layer was attached to a metakaolin substrate. Evidence of mechanical interlocking is presented in Figure 6b. The reaction area between the A1100 alloy and the metakaolin substrate was promoted by this phenomenon. Its average thickness was 0.91 microns. This thin and continuous layer provided thermal conductivity.

Joining the AA1100 alloy and metakaolin substrate by friction base joining was by a solid-state joining technique [32, 33]. Therefore, the temperature should be lower than the melting point of the AA1100 alloy. The temperature profile during the holding time is plotted in Figure 7. The graph can be divided into 4 stages. The first stage is from 1-5 sec. This is the initial deformation state where the temperature of the consumable rod slightly increased, but was nearly constant. From 5-7 sec, the temperature increased rapidly to 261 ℃ and deformed Al flow occurred. Then, from 7-9 sec, deposition of the coating process occurred. Finally, from 9-10 sec, the temperature of the consumable rod cooled rapidly to 62 ℃. Although the deposition period was very short, the maximum temperature of the AA1100 surface during coating was 261 ℃, approximately $0.4T_m$, which is lower than the recrystallization temperature of aluminium ($0.6T_m$ or ~300 ℃). This guarantees softening of Al and capability of being deposited on metakaolin. So, the AA1100 rod underwent a cold working process when pressure and shear force were applied.

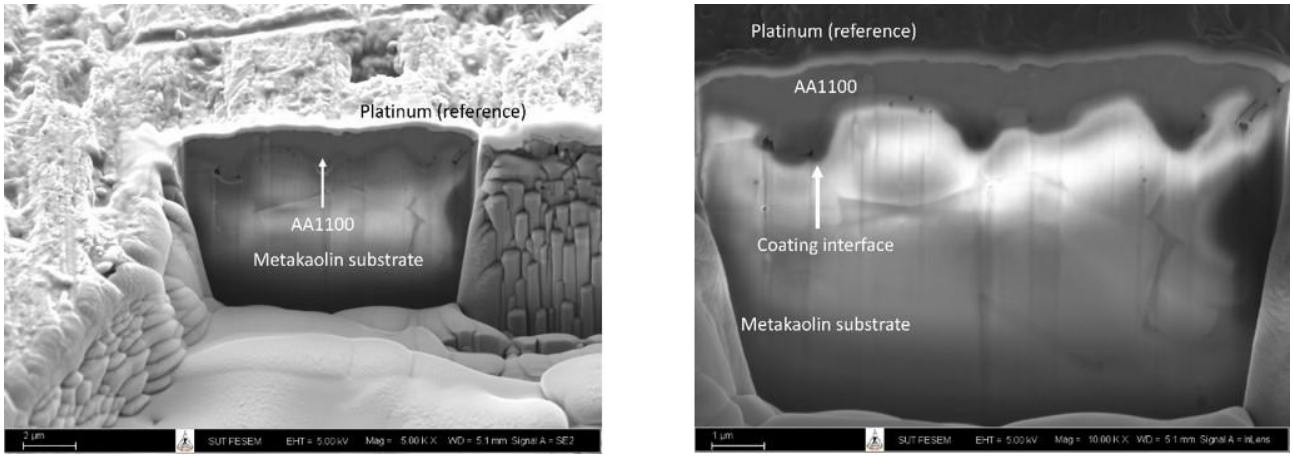

(a) (b)

Figure 6 (a) FIB-FESEM Image at a 5,000x magnification of a selected area showing the thickness of the spot friction surface coating layer, (b) FIB-FESEM Image at a 10,000x magnification of a selected area showing the thickness of the spot friction surfacing coating layer.

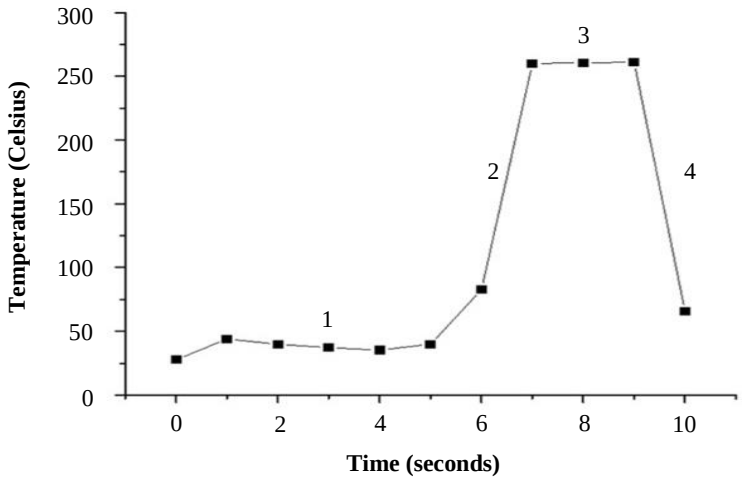

Figure 7 Relationship between coating temperature and friction time.

The impact of temperature on the coating material was evidence of a stick-slip phenomenon [34]. Stick-slip produces vibration, heat and sound. The difference in the kinetic friction force generated at the interface between the consumable rod and the metakaolin substrate was also a stick-slip phenomenon. When a kinetic friction force is increased, frictional heat increases. Conversely, when kinetic friction force decreases, frictional heat also decreases. So, an indicator of kinetic friction force is the process temperature.

According to Bedford GM, et al., Rafi HK, et al. and Gandra J, et al. [29-31], a thermomechanical process occurs due to the effect of the kinetic friction force that is generated by compression and shear stress. When the consumable rod at the interface is deformed by compression and shear stress, a kinetic friction force is generated and observed in terms of frictional heat. Aluminium at the tip of a consumable rod exhibits a plastic deformation and begins to flow. This behavior is known as viscoplasticity. Additionally, a period of sticking in a stick-slip phenomenon occurs in this process. After the viscoplastic layer of the aluminium consumable rod has slipped and deposited itself on the planar metakaolin substrate, the area of coating layer increases. The most frictional heat, generated by compression and shear stress, was transferred to the coated layer. Additionally, the kinetic friction force and the process temperature decreased.

3.2 Electrical resistance

The results of electrical resistance measurement of the coating layer across 10 lines: C-1, D-C, D-1, B-D, B-C, B-1, A-1, A-D, A-C and A-B of two overlapping spots are presented in Table 3. The electrical resistance values were uniform in all directions. This is evidence of a continuous AA1100 coating. The average electrical resistance was 0.3266 Ω. Electrical resistances lower than 1 Ω are suitable for various electrical applications.

Table 3 Electrical resistance of AA1100 coating layer

Position	AB	AC	AD	A1	B1	BC	D1	AC	C1	Average
Resistance (Ω)	0.374	0.452	0.228	0.331	0.395	0.265	0.333	0.297	0.265	0.3266

3.3 Mechanical properties

3.3.1 Residual stress

Using the conventional d-sin^{2}Ψ method, 2θ angles and the intensity of the incident angle were plotted and aligned as presented in Figure 8. According to the relationship between 2θ and the intensity of the incident angle, the group of sin^2 ψ data and length of the unit cell (a) data were extracted and generated in terms of a scatter plot. The linear correlation of the scatterplot was also calculated.

After that, slope and y-intercept values were extracted and used to calculate residual stress, as presented in Figure 9. Residual stress was generated in every condition of the lattice plane. However, since the residual stress, which was calculated from the lattice plane with low diffraction angles was variable and had extraordinarily high values, the lattice plane with a high diffraction angle should be considered [28]. In this study, the 311 lattice plane had a high diffraction angle. The value of residual stress calculated from this plane was-27.20 MPa. So, this indicates shrinkage of the aluminum coating layer. Compression stress was generated by this phenomenon. This result agrees with the work done by Hsueh CH and Evans AG. [6]. Furthermore, since the yield strength of the aluminum and the process temperature are low, the residual stress generated from spot friction surfacing was also low and expansion of the aluminium coating layer was reduced. Thus, the likelihood of cracking the metakaolin substrate by residual stress was low. Additionally, residual stress of the coating layer varied directly with layer thickness [35]. So, a thinner coating layer reduced the residual stress.

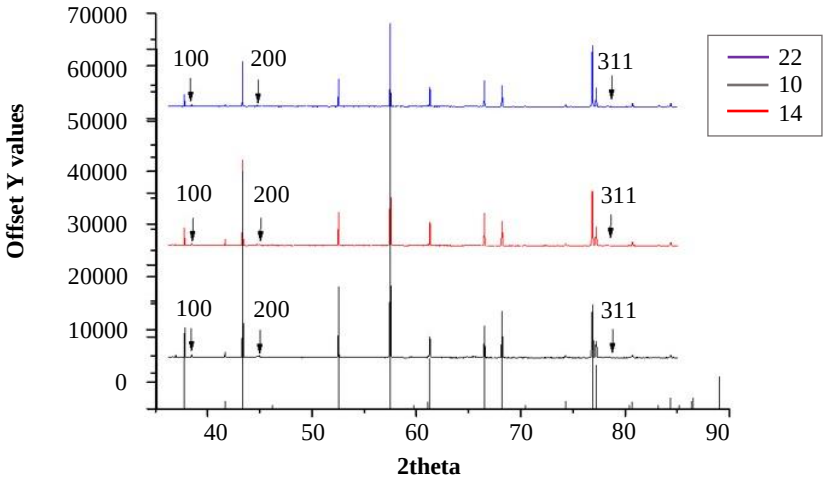

Figure 8 X-ray diffraction of aluminium coating layer.

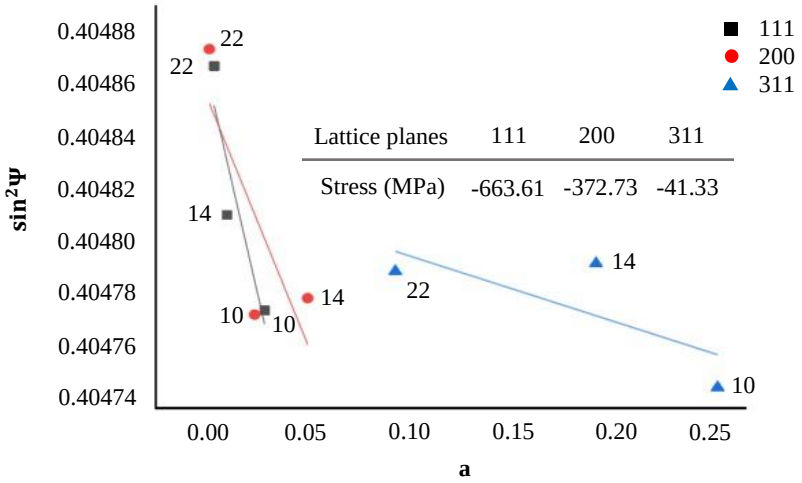

Figure 9 Sin^2 Ψ values vs. length of unit cell (a) plots from various lattice planes of aluminium coating layers calculated under the conventional d-sin^{2}Ψ mode.

3.3.2 Hardness and Young's modulus

From the nanoindentation tests, the as-received AA1100 alloy had an average hardness of 0.508 GPa, standard deviation of 0.019 GPa and an average hardness of the aluminium coating layer of 2.03 GPa, with a standard deviation of 0.66 GPa. The increased hardness of the AA1100 coating layer was 299.60% more than the as-received AA1100 alloy. It can be clearly seen that the aluminium AA1100 coating layer was harder than the as-received aluminium. This indicates a cold working process. Many studies have reported about hot working processes and recrystallization in the friction surfacing process [36-38]. However, in this study, since the structure of aluminium is FCC and has a high stacking fault energy (~170 mJ m^{-2}) [39], when aluminium is deformed, the recovery of dislocation was rapid and continuous, resulting in a low internally stored energy. Aluminium AA1100 is a highly ductile material, so recrystallization of aluminium does not occur during the process. Additionally, the high hardness of aluminium means that dislocation densities after deformation in the cold working process remain high. This implies that the coating layer has high a dislocation density after deformation, leading to an increase in electrical resistivity [40, 41]. Additionally, the disparate hardness values did not alter the Young's modulus of the aluminium alloy. The calculated Young's modulus of the initial rod and the coating layer were 68.48 GPa and 69.99 GPa, respectively.

3.4 Degree of failure

The average surface roughness (Rz) of the pre-process metakaolin substrate was 3.71 microns, with a standard deviation of 0.017 microns. Average surface roughness (Rz) of the post-process metakaolin substrate was 3.129 microns with a standard deviation of 0.356 microns. The reduction of Rz of the post-process metakaolin substrate was 15.66% of the pre-process substrate. Therefore, the post-process metakaolin substrate was slightly worn by friction. Additionally, the microstructure of the pre-process and post-process metakaolin substrates are compared in Figure 10. There is no evidence of micro-or macro-cracking on the post-process metakaolin substrate. In the current study, the spot friction surfacing process with its experimental conditions did not cause failure of the metakaolin substrate.

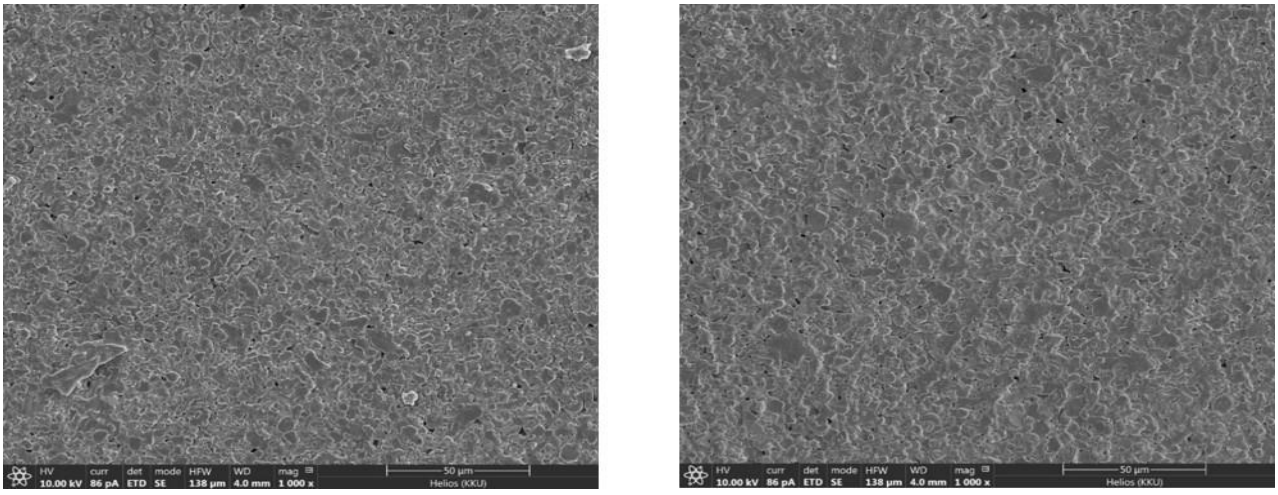

(a) (b)

Figure 10 SEM Images of (a) initial metakaolin substrate, (b) post-process metakaolin substrate.

4. Conclusion

Spot friction surfacing temperature evolution can be divided into four stages, an initial deformation where temperature is nearly constant, flow of Al as temperature rapidly increases, deposition at a constant temperature and cooling as temperature rapidly drops. A related stick-slip phenomenon was observed. The maximum temperature of the AA1100 surface during coating was 261 ℃, which is lower than the recrystallization temperature of the AA1100 alloy.

Aluminum AA1100 was successfully deposited on a metakaolin substrate *via* a spot friction surfacing process. The aluminium coated layer adhered continuously to the metakaolin substrate with no cracking. Mechanical interlocking was observed. There was no evidence of macro-or micro-cracking on the post-process substrate due to the friction surfacing process. The Rz of the post-process substrate was 15.66% less than the pre-processed substrate.

Residual stress varies directly with the strength of a material. The strength of a soft material and 0.91 micron thin layer of Aluminum AA1100 was low. For this reason, the residual stress of the Al 1100 coating layer was low. The electrical resistance values of the Aluminum 1100 coating layer were low and uniform in all directions of measurement. These results support the evidence of a continuous AA1100 coating layer.

The value of compressive residual stress calculated by the conventional method from the 311 planes of the AA1100 coated layer was-27.20 MPa. The hardness of the aluminium AA1100 of the coating layer was 299.60% higher than that of the as-received aluminium AA1100 alloy. Therefore, the cold working process was the major deformation mechanism in this study. From the evidence, spot friction surfacing can be applied in the production of DBA substrates.

5. Acknowledgements

This research was supported by a Khon Kaen University Research Grant (KKU-Syn2561-009)

6. References

[1] He H, Fu R, Wang D, Song X, Jing M. A new method for preparation of direct bonding copper substrate on Al_2O_3. Mater Lett. 2007;61(19-20):4131-3.
[2] Mouawad B, Thollin B, Buttay C, Dupont L, Bley V, Fabregue D, et al. Direct copper bonding for power interconnects: design, manufacturing, and test. IEEE Trans Compon Packag Manuf Technol. 2014;5(1):143-50.
[3] Schulz-Harder J. Advantages and new development of direct bonded copper substrates. Microelectron Reliab. 2003;43(3):359-65.
[4] Arai K, Nishimoto S, Romanjek K, Komasaki M, Nagatomo Y, Kuromitsu Y. Development of high-durability substrates for thermoelectric modules. J Electron Mater. 2019;48:1976-80.
[5] Wang YT, Cheng YH, Lin CC, Lin KL. Direct bonding of aluminum to alumina using a nickel interlayer for power electronics applications. Results Mater. 2020;6:100093.
[6] Hsueh CH, Evans AG. Residual stresses in metal/ceramic bonded strips. J Am Ceram Soc. 1985;68(5):241-8.
[7] Dong G, Chen X, Zhang X, Ngo KD, Lu GQ. Thermal fatigue behaviour of Al_2O_3-DBC substrates under high temperature cyclic loading. Solder Surf Mt Technol. 2010;22(2):43-8.
[8] Camilleri D. Thermo-mechanical behaviour of DBC substrate assemblies subject to soldering fabrication processes. Solder Surf Mt Technol. 2012;24(2):100-11.
[9] Yamada T, Yokoi K, Kohno A. Effect of residual stress on the strength of alumina-steel joint with Al-Si interlayer. J Mater Sci. 1990;25:2188-92.
[10] Suganuma K. Chapter 10.1. Joining ceramics and metals. In: Somiya S, editor. Handbook of advanced ceramics: 2nd ed. Amsterdam: Academic Press; 2013. p. 775-88.
[11] Lei TG, Calata JN, Ngo KDT, Lu G. Effects of large-temperature cycling range on direct bond aluminum substrate. IEEE Trans Device Mater Reliab. 2009;9(4):563-8.
[12] Kraft S, Schletz A, Maerz M. Reliability of silver sintering on DBC and DBA substrates for power electronic applications. Conference on Integrated Power Electronics Systems (CIPS); 2012 Mar 6-8; Nuremberg, Germany. New York: IEEE; 2012. p. 1-6.
[13] Mitic G, Licht T, Lefranc G. IGBT Module technology with high partial discharge resistance. Conference Record of the 2001 IEEE Industry Applications Conference 36th IAS Annual Meeting; 2001 Sep 30-Oct 4; Chicago, USA. New York: IEEE; 2001. p. 1899-904.
[14] Richter J, Schellscheidt B, Steenmann A, Licht T. Comparison of electroplated Ni and PVD Ni coating layers after soft soldering process. Key Eng Mater. 2019;809:367-71.
[15] Lee SK, Lee JH, Kim YH. Nucleation and growth of zinc particles on an aluminum substrate in a zincate process. J Electron Mater. 2007;36(11):1442-7.
[16] Md Arshad MK, Ahmad I, Jalar A, Omar G, Hashim U. The effects of multiple zincation process on aluminum bond pad surface for electroless nickel immersion gold deposition. J Electron Packag. 2005;128(3):246-50.
[17] Schwartz MM. Ceramic joining. USA: ASM International; 1990.
[18] Noh MZ, Hussain LB, Ahmad ZA. Alumina-mild steel friction welded at lower rotational speed. J Mater Process Technol. 2008;204(1-3):279-83.
[19] Seli H, Noh MZ, Ismail AI, Rachman E, Ahmad ZA. Characterization and thermal modelling of friction welded alumina-mild steel with the use of Al 1100 interlayer. J Alloys Compd. 2010;506(2):703-9.
[20] Mingmuang T, Lee S, Thinvongpituk C. Mechanical properties of aluminium-alumina welding by friction welding. Adv Mat Res. 2011;418-420:1279-87.
[21] Gandra J, Krohn H, Miranda RM, Vilaça P, Quintino L, dos Santos JF. Friction surfacing-a review. J Mater Process Technol. 2014;214(5):1062-93.
[22] Akbari M, Asadi P. Optimization of microstructural and mechanical properties of friction stir welded A356 pipes using Taguchi method. Mater Res Express. 2019;6(6):066545.
[23] Mingmuang D, Talangkun S, Paengson S, Seetawan T. Thermoelectric cell produced from AA1100 aluminium alloy coating on metakaolin by friction surfacing process. Mater Sci Forum. 2019;947:130-4.
[24] Vellvehi M, Perpiñà X, Lauro GL, Perillo F, Jordà X. Irradiance-based emissivity correction in infrared thermography for electronic applications. Rev Sci Instrum. 2011;82(11):114901.
[25] Hardiman M, Vaughan TJ, McCarthy CT. A review of key developments and pertinent issues in nanoindentation testing of fibre reinforced plastic microstructures. Compos Struct. 2017;180:782-98.
[26] Srinivas T, Reddy AC. Finite element analysis of warm deep drawing process for rectangular cup of AA1100 aluminum alloy. Int J Curr Adv Res. 2015;3(6):1383-91.
[27] Klein CA. Anisotropy of Young's modulus and Poisson's ratio in diamond. Mater Res Bull. 1992;27(12):1407-14.
[28] Luo Q, Yang S. Uncertainty of the x-ray diffraction (XRD) sin2 ψ technique in measuring residual stresses of physical vapor deposition (PVD) hard coatings. Coatings. 2017;7(8):128.
[29] Bedford GM, Vitanov VI, Voutchkov II. On the thermo-mechanical events during friction surfacing of high speed steels. Surf Coat Technol. 2001;141(1):34-9.
[30] Rafi HK, Balasubramaniam K, Phanikumar G, Rao KP. Thermal profiling using infrared thermography in friction surfacing. Metall Mater Trans A. 2011;42(11):3425-9.
[31] Gandra J, Miranda RM, Vilaça P. Performance analysis of friction surfacing. J Mater Process Technol. 2012;212(8):1676-86.
[32] Ahmad Fauzi MN, Uday MB, Zuhailawati H, Ismail AB. Microstructure and mechanical properties of alumina-6061 aluminum alloy joined by friction welding. Mater Des. 2010;31(2):670-6.
[33] Uday MB, Ahmad-Fauzi MN, Noor AM, Rajoo S. Current issues and problems in the joining of ceramic to metal. In: Ishak M, editor. Joining technologies. London: IntechOpen; 2016. p. 159-93.
[34] Jiménez AE, Bermúdez MD. Friction and wear. In: Davim JP, editor. Tribology for engineers. Sawston; Woodhead Publishing; 2011. p. 33-63.
[35] Zhang S, Yang H, Gao K, Yan L, Pang X, Volinsky AA. Residual stress and warpage of AMB ceramic substrate studied by finite element simulations. Microelectron Reliab. 2019;98:49-55.

[36] Vilaça P, Gandra J, Vidal C. Linear friction-based processing technologies for aluminum alloys: surfacing, stir welding and stir channeling. In: Ahmad Z, Editor. Aluminium alloys: new trends in fabrication and applications. Rijeka: InTech; 2012. p. 159-98.
[37] Tokisue H, Katoh K, Asahina T, Usiyama T. Mechanical properties of 5052/2017 dissimilar aluminum alloys deposit by friction surfacing. Mater Trans. 2006;47(3):874-82.
[38] Thomas WM. An investigation and study into friction stir welding of ferrous-based material [dissertation]. Bolton: University of Bolton; 2009.
[39] Polmear I, StJohn D, Nie JF, Qian M. Light alloys: metallurgy of the light metals. 5th ed. Oxford: Elsevier; 2017.
[40] Kovács-Cseténvi E. Electrical resistivity change in cold-worked tungsten wires during recovery and recrystallization. Acta Phys Acad Sci Hung. 1964;18(1):11-8.
[41] Miyajima Y, Komatsu SY, Mitsuhara M, Hata S, Nakashima H, Tsuji N. Change in electrical resistivity of commercial purity aluminium severely plastic deformed. Philos Mag. 2010;90(34):4475-88.